Immobilization capacity assessment of a binder from arsenic-containing biohydrometallurgy waste

Effects of halloysite nanotubes and biochar addition

Zhao, Yingliang; Sun, Yong; Guo, Zhenbang; Sun, Xiaogang; Qiu, Jingping

DOI
10.1016/j.scitotenv.2023.164637

Publication date
2023

Document Version
Final published version

Published in
Science of the Total Environment

Science of the Total Environment 891 (2023) 164637

Contents lists available at ScienceDirect

Science of the Total Environment

journal homepage: www.elsevier.com/locate/scitotenv

Immobilization capacity assessment of a binder from arsenic-containing biohydrometallurgy waste: Effects of halloysite nanotubes and biochar addition

Yingliang Zhao [a,b], Yong Sun [a], Zhenbang Guo [a,c], Xiaogang Sun [a], Jingping Qiu [a,*]

[a] College of Resources and Civil Engineering, Northeastern University, Shenyang, China
[b] Department of Civil and Environmental Engineering, The Hong Kong Polytechnic University, Kowloon, Hong Kong
[c] Faculty of Civil Engineering and Geosciences, Department of Hydraulic Engineering, Delft University of Technology, Delft, the Netherlands

HIGHLIGHTS

- Both HNTs and BC could effectively increase the immobilization capacity of BAW for As.
- Higher dosage of BC strongly decreased the early age strength of BAW.
- Adding HNTs enhanced the physical encapsulation capacity for As.
- As species could be adsorbed onto the surface of HNTs via formation of H-bonds.

GRAPHICAL ABSTRACT

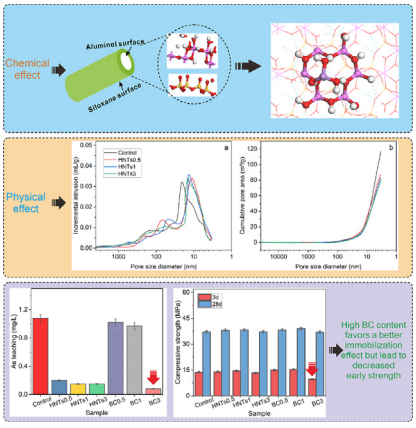

ARTICLE INFO

Editor: Daniel CW Tsang

Keywords:
Biohydrometallurgy waste
As immobilization
Leaching characteristics
Density function theory

ABSTRACT

The aim of this study was to improve the immobilization capacity of a binder prepared from As-containing biohydrometallurgy waste (BAW) on arsenic (As) by modifying it with halloysite nanotubes (HNTs) and biochar (BC). The study investigated the influence of HNTs and BC on the chemical fractions and leaching characteristics of As, as well as the influence on the compressive strength of BAW. The results indicated that the addition of HNTs and BC effectively decreased As leaching. The presence of 1.0 wt% HNTs decreased the As leaching concentration from 1.08 mg/L to 0.15 mg/L, with the corresponding immobilization rate reaching about 90.9 %. A high amount of BC seemed to show better performance in improving the As immobilization capacity of BAW. However, a strongly reduced early compressive strength of BAW was observed, making it unsuitable to be used as an additive in this situation. The effects of HNTs on the increase of As immobilization capacity of BAW were attributed to two aspects. Firstly, As species were adsorbed onto the surface of HNTs via H-bonds, which was verified via density functional theory calculation. Secondly, the addition of HNTs decreased the pore volume of BAW, leading to a more compact structure, and hence increasing the physical encapsulation capacity for As.

Environmental implication: The rational disposal of arsenic-containing biohydrometallurgy waste has always been a top priority for the green and low-carbon development of the metallurgical industry. In this article, we have taken the perspective of large-scale resource utilization of solid waste and pollution control, and developed arsenic-containing

* Corresponding author.
E-mail address: qiujingping@mail.neu.edu.cn (J. Qiu).

http://dx.doi.org/10.1016/j.scitotenv.2023.164637
Received 25 March 2023; Received in revised form 7 May 2023; Accepted 1 June 2023
Available online 7 June 2023

biohydrometallurgy waste into a cementitious material, and enhancing arsenic immobilization capacity with the addition of HNTs and BC. This study provides an effective method for the rational disposal of arsenic-containing biohydrometallurgy waste.

1. Introduction

The World Health Organization has identified arsenic (As) as a human carcinogen (Basu et al., 2001; Phenrat et al., 2008; Straif et al., 2009; Stueckle et al., 2012), and it is often found alongside other non-ferrous metals like lead, zinc and nickel (Zhao et al., 2022a). In ores containing As, valuable elements are typically in the form of small inclusions combined with As-bearing minerals, which lowers the recovery rate (Lin et al., 2022). Therefore, some As-containing ores require pre-treatment to extract valuable elements (Nunan et al., 2017). The most common method of treating As-containing ores is biohydrometallurgy, which uses microorganisms as catalyst (Arrascue and van Niekerk, 2006; Brierley, 2003; Langhans et al., 1995). As is dissolved and released into the solution during this process. However, the biohydrometallurgy method produces a large amount of As-containing acidic wastewater (AAW) that can cause severe environmental pollution (Li et al., 2020). Furthermore, when non-ferrous metals like copper, nickel, lead, zinc, etc., undergo pyrometallurgical smelting, some of the As is removed through washing and purification of the flue gas before the production of acid, leading to As entering the washing wastewater (Che et al., 2022; Zhang et al., 2021). Eventually, it also leads to the creation of a significant amount of AAW. In China, for example, the copper smelting process alone produces 12 million m^3 of AAW each year (Li et al., 2020).

AAW is highly acidic and contains significant amounts of As (the content of H_2SO_4 up to 10–80 g/L, the content of As up to 4–30 g/L), making it unsuitable for direct use or discharge. As a result, there is global interest in treating this type of wastewater. The most commonly used method for treating AAW in industries is the lime/calcite-ferrate process due to its cost-effectiveness and simplicity (Peng et al., 2017). Neutralization precipitation using limestone or lime is used to remove As from the wastewater, but it generates a large amount of As-containing waste (AW) that requires proper disposal. For every cubic meter of AAW treated using the lime/calcite-ferrate method, approximately 70 kg of AW is produced (Guo et al., 2015). AW is unstable and prone to As leaching, which can lead to secondary pollution (Lagno et al., 2010). Therefore, the safe and proper disposal of AW is a matter of global concern.

There are several methods available for treating As-containing waste (AW), including solidification with cement, stabilization with nanomaterials (Sun et al., 2021), hydrothermal treatment (Xu et al., 2020), gypsum preparation (Yang et al., 2019b), and soil amendments (Yang et al., 2019a). While these methods can reduce the harmful effects of AW to some extent, they tend to have limitations such as low efficiency, high costs, and poor volume reduction. AW has a high concentration of calcium sulfate, which makes it a potential candidate for producing super sulfated cement (SSC). SSC is considered an effective substitute for ordinary Portland cement (OPC) due to its eco-friendly and economical properties (Mehrotra et al., 1982). In previous research, we successfully prepared a binder (Fig. 1) using AW as the main raw material (Zhao et al., 2022b, 2022c; Zhao et al., 2022d).

The ability to immobilize As in a prepared binder is an important factor to be considered. The effectiveness of the binder in immobilizing hazardous elements is dependent on both physical and chemical factors (Chen et al., 2023; Guo et al., 2017). Physical factors involve encapsulating the hazardous elements in a compact structure, preventing the diffusion of hazardous elements (Malviya and Chaudhary, 2006; Randall and Chattopadhyay, 2004). Chemical factors involve the reaction between hazardous elements and cementitious materials, resulting in the formation of relatively insoluble, low-toxicity substances (Chrysochoou and Dermatas, 2006; Wang and Wang, 2022). For instance, studies have shown that calcium chromate precipitation can be formed when Cr(VI) reacts with Ca^{2+} in the cementitious reaction system, which reduces the leaching concentration of Cr(VI) (Zhang et al., 2018). Moreover, the components of cementitious materials and the series of gels produced during the reaction can have a chemical stabilizing effect on hazardous elements through surface adsorption and/or ion substitution (Avalos et al., 2021; Baldermann et al., 2021; Gillispie et al., 2021).

Utilization of additives to increase the immobilization capacity of a binder is a feasible method (Alias et al., 2020; Cao et al., 2017; Dandautiya et al., 2018; Gong et al., 2022; Halim et al., 2003; Hamid et al., 2020; Mahallei and Badv, 2021; Ouhadi et al., 2021; Quedou et al., 2021; Wang et al., 2022; Zhang et al., 2022a). In the research by Cao et al. (Cao et al., 2017), binders were modified with hematite nanoparticles to enhance uranium immobilization; the results showed that the slowest uranium leaching was found in the samples with 1.0 % hematite nanoparticles. The increase in the immobilization capacity was attributed to uranium adsorption onto hematite nanoparticles and the refinement in pore structure by hematite nanoparticles, according to the illustrations by the authors (Cao et al., 2017). Similar immobilization effects of ferrihydrite

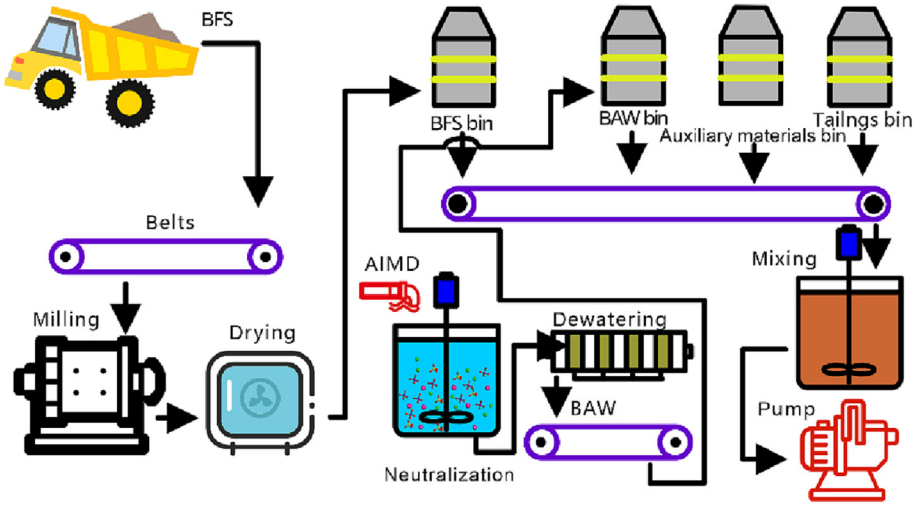

Fig. 1. Production procedure for BAW.

nanoparticles on uranium, strontium and cesium have also been reported (Fan et al., 2019). While using these nano-particles should consider some problems like cost and safety.

Halloysite nanotubes (HNTs) consist of a naturally occurring 1:1 tubular clay mineral that includes one tetrahedral (Si—O) sheet and one octahedral (Al-OH) sheet. HNTs offer numerous advantages, such as high cation exchange capacity, high aspect ratio, high surface area, excellent thermal stability, and good biocompatibility. These unique properties make HNTs an exceptional adsorbent for water treatment, and they have been successfully used in environmental remediation (Cataldo et al., 2018; Emmanuel et al., 2020; Li et al., 2018).

Additionally, biochar (BC) is a carbon-rich and porous substance that is produced from the pyrolysis of waste biomass. It has been proven to have a significant sorption capacity for both inorganic and organic pollutants (Mohanty et al., 2018; Wang et al., 2019; Yu et al., 2019). Kushwaha et al. (2023) investigated the effects of BC on As toxicity in soybean plants; the results showed that the addition of BC reduced As bioavailability and offset its negative effect on plant growth (Kushwaha et al., 2023). The FTIR results indicated that the presence of O-containing groups on the BC surface act as sites for the complexation of As to produce insoluble complex and enhances the As-sorption (Kushwaha et al., 2023). Similarly, Dias et al. (Dias et al., 2022) found that the addition of BC in gold mine tailings reduced the bioavail0ability of As. On the other hand, previous works also indicated that the addition of BC could increase the binding properties of a binder and achieve carbon neutrality (Chen et al., 2022; He et al., 2022; Zhang et al., 2022b). The porous structure and functionalized surface of BC could provide nucleation sites for binder reaction (He et al., 2022), and show internal curing effect (Chen et al., 2022), which will then enhance the immobilization efficiency. Moreover, severe greenhouse gas emissions and environmental pollution issues have been caused by biomass waste, which is the raw materials for BC production. The transformation of biomass into BC provide a feasible strategy for long-term decarbonization and promote a circular economy (He et al., 2022).

Although the superior removal capacity of HNTs and BC for hazardous substances is well-known, limited research has been conducted on their effects when used as additives in cementitious materials. This is because their effects are related to the balance between the immobilization effects on hazardous elements and the influence on binder hydration. In the present study, HNTs and biochar BC were used as additives to modify the As immobilization capacity of a binder prepared by AW. The effect of HNTs and BC on As leaching characteristics was investigated via toxicity characteristic leaching procedure (TCLP) and semi-dynamic leaching. At the same time, the influence of HNTs and BC on the strength development and reaction products of the binder was also investigated. Additionally, density function theory calculation was used to explain the chemical stabilization effects of the additives on As.

2. Materials and methods

2.1. Materials

The raw materials used in this experiment included arsenic-containing biohydrometallurgy waste (AW), blast furnace slag (BFS), ordinary Portland cement (OPC), carbide slag (CS), aluminum sulfate (AlS), as well as halloysite nanotubes (HNTs) and biochar (BC).

AW used in this study was taken from the San Dao Gou gold mine in Fengcheng, Liaoning Province. The chemical composition of AW was shown in Table S1. As can be seen from Table S1, its chemical composition was mainly composed of CaO, SO_3, and Fe_2O_3, which together accounted for >76 wt% of the total. In addition, the content of As_2O_3 in the AW was as high as 1.48 wt%, which was highly soluble and can cause environmental pollution. The phase composition of AW was shown in Fig. S1a, which was mainly β-semi-hydrated gypsum, followed by a small amount of dihydrate gypsum and anhydrous gypsum.

BFS was provided by Shandong Panlongshan Material Co., Ltd. It was a S95 grade slag powder, and its chemical composition was shown in Table S1. According to the chemical composition of BFS, its alkaline coefficient was 1.02 according to GB/T 203–2008. The phase composition of BFS was shown in Fig. S1c. BFS was mainly amorphous, with only a small amount of gehlenite. The particle size distribution curve of BFS showed that its d10, d50, and d90 are 1.88 μm, 11.20 μm, and 31.30 μm, respectively. The cement was produced by China Resources Cement Co., Ltd., and its chemical composition was shown in Table S1.

CS was provided by Xinyu Materials Company in Lingshou, Hebei province, and its chemical composition was shown in Table S1. As indicated in Table S1, CaO was the major component of the CS, accounting for >95 wt %. The phase composition and particle size distribution of the electric furnace slag were shown in Fig. S1e and f, respectively. Fig. S1e showed that the main phase in the CS was calcium hydroxide. Fig. S1f showed that the particle size distribution of the CS and the content of particles smaller than 74 μm was approximately 78 %.

HNTs was purchased from Yanbo Mineral Processing Plant in Hebei province and the chemical compositions were shown in Table S1. According to Table S1, the chemical composition of HNTs was mainly SiO_2 and Al_2O_3, accounting for >93 wt% of the total.

BC were purchased from Nanjing Zhironglian Technology Co., Ltd. According to the provider, BC was produced under no-oxygen conditions. Air dried straw was cut into small segments with the length around 10 cm and fed into the BC reactor. After that, the reactor was heated to 500 °C using a rate of 8.5 °C/min and maintained for about 10 h. Subsequently, the heating system was cut off and cooled to room temperature. The obtained BC was ground before being used in the present work. The chemical composition of BC (Table S1) was mainly C, SiO_2, and K_2O, accounting for approximately 85 wt% of the total.

The XRD analysis results of HNTs and BC were shown in. Fig. 2a and b showed that the main phase of HNTs was halloysite, while the main phase of BC was amorphous, with small amounts of SiO_2 and $KCaSiO_4$. The particle size distributions of HNTs and BC were shown in Fig. 2c and d, respectively, and their particle sizes are generally smaller than 74 μm. The FTIR results of BC were shown in Fig. 2e. It can be seen that the surface of BC was abundant in C—O, C═C and C—H, which could form complexes and hydrogen bonds with As species (Sharma et al., 2022). According to BET results (Fig. 2f), BC had highly porous structure and its pore diameter ranged from 2 to 100 nm, and the cumulative surface area of pores was 11.4638 m^2/g. The porous structure of BC could provide more active adsorption sites for hazardous elements.

The microstructures of HNTs and BC are shown in Fig. 3, which showed that the microstructure of HNTs was rod-like, while the microstructure of BC was porous, resulting in its higher adsorption activity.

2.2. Methods

2.2.1. Sample preparation

According to the proportions listed in Table S2, the raw materials were pre-mixed for 2 min using a cement slurry mixer. Water (liquid-solid ratio of 0.5) was then added and mixed for 5 min to ensure that the slurry was evenly mixed. The slurry was then poured into cylindrical molds measuring 50 mm × 100 mm and 5 mL centrifuge tubes. After that, the samples were placed in a curing box and cured at 20 ± 1 °C and 95 % relative humidity until the designated age. The cylindrical samples were mainly used to test the uniaxial compressive strength and leaching characteristics of the samples, while the samples in the 5 mL centrifuge tubes were used to test the phase composition and microstructure of the samples.

2.2.2. Sequential extraction procedure

The chemical fractions of As were determined by using the sequential extraction procedure specified in GBT 25282–2010. The testing procedure is shown in Fig. S2.

2.2.3. Toxicity characteristic leaching procedure

The total amount of As in the sample was tested using the HNO_3-HF-HCl digestion method. 0.2 g of the sample was weighed and placed in a mixed

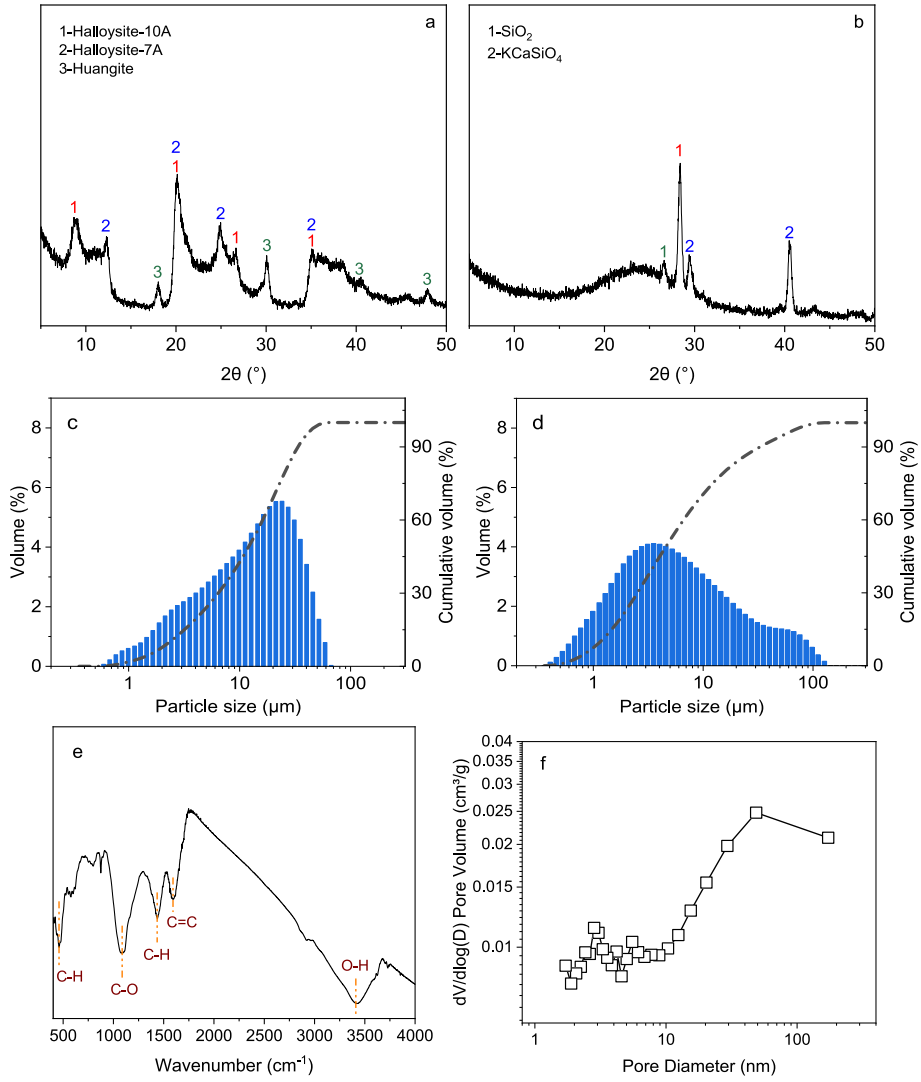

Fig. 2. XRD patterns and particle size distribution of the raw materials: HNTs (a, c), BC (b, d), FTIR (e) and BET (f) results of biochar.

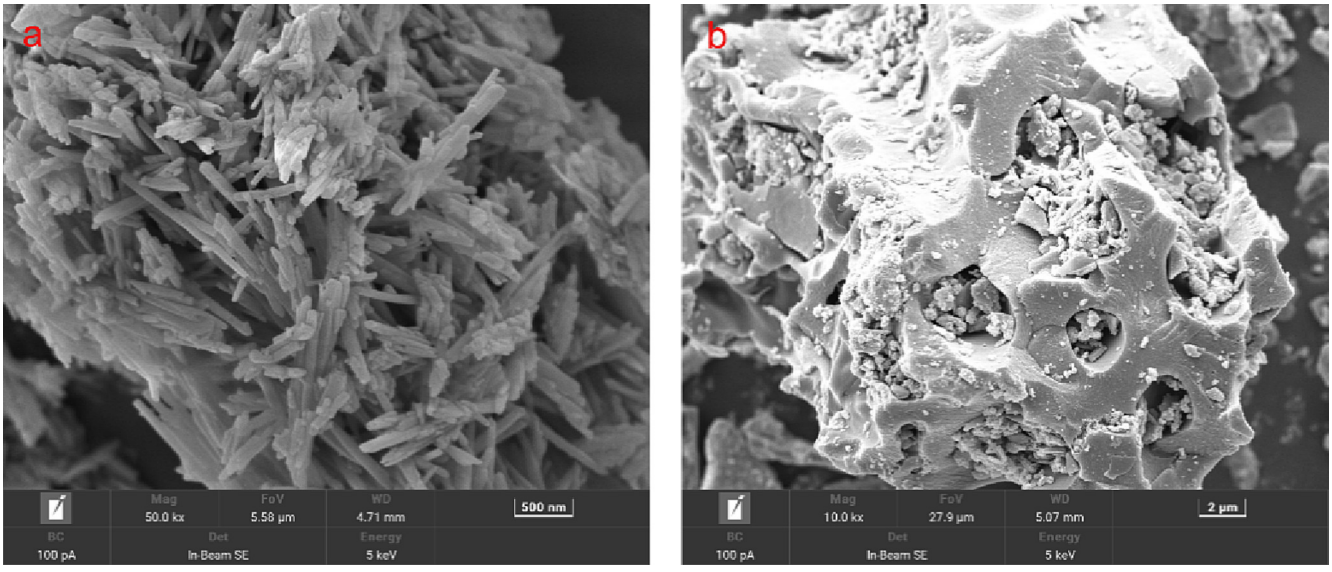

Fig. 3. Microstructure of the raw materials: (a) HNTs, (b) BC.

solution of 6 mL HNO_3, 2 mL HCl, and 2 mL HF. The mixture was then digested in a microwave digestion instrument at 140 °C. After cooling, the solution was filtered using a 0.45 μm filter membrane, and the content of harmful elements was determined using an inductively coupled plasma mass spectrometer.

The toxicity characteristic leaching procedure (TCLP) was tested according to the GB HJT 300–2007 (HJ 557–2010, 2010) using a horizontal shaking method. 10 g ± 0.1 g of the sample was mixed with 200 mL of acetic acid (pH = 2.64 ± 0.05) and placed in a 1 L conical flask. The mixture was shaken horizontally for 18 h using a horizontal shaker at 23 ± 3 °C. The solution was then filtered using a 0.45 μm filter membrane, and the content of As in the filtrate was determined. The immobilization ratio (IR) of arsenic can be calculated using Eq. (1):

$$IR = \left(1 - \frac{CV}{M}\right) \times 100\% \quad (1)$$

where, C is the As concentration in the leachate, mg/L.

V is the volume of leaching solution, L.

M is the total As content in the samples, mg.

2.2.4. Semi-dynamic leaching

The semi-dynamic leaching test method was performed following the method described by Irisawa et al. (Irisawa et al., 2022). The sample was suspended in the center of the leaching solution after curing for 28 days. Distilled water (with a ratio of 10 mL/cm^2 of sample surface area) was used as the leaching solution. The experiment was conducted at 20 ± 1 °C, and the leachate was collected and replaced at 2 h, 7 h, 1 d, 2 d, 3 d, 4 d, 14 d, 28 d, 43 d, and 91 d. The content of As in the leachate was measured after filtrating.

The diffusion coefficient (D_e, cm^2/s) was obtained using Eqs. (2) and (3) (Irisawa et al., 2022).

$$CFL = \frac{2S}{V}\sqrt{\frac{D_e t}{\pi}} \quad (2)$$

$$D_e = \frac{\pi}{4}\left(\frac{V}{S}\right)^2 \frac{CFL^2}{t} \quad (3)$$

where, CFL was cumulative fraction leached.

V was the samples volume, m^3.

S was the samples' surface area, m^2.

t was the leaching duration, s.

The leachability index (LI) could be calculated from the cumulative D_e, as shown in Eq. (4) (Zhang et al., 2020).

$$LI = \left(\frac{1}{m}\right)\Sigma_{n=1}^{n=m}(-\log(D_e))_n \quad (4)$$

where, n was number of leaching cycles, n = 1–10.

m was the total leaching cycle, m = 10.

By analyzing the $log(M_t)$-$log(t)$ diagram's slope, it is possible to determine the leaching mechanism of As, as shown in Eq. (5).

$$log\ (M_t) = \frac{1}{2}\ log\ (t) + log\left(Q_0 d\sqrt{\frac{D_e}{\pi}}\right) \quad (5)$$

where, M_t was the cumulative As release, mg/m^2.

Q_0 was the total amount of As in the sample, mg/kg.

d was the volume density of sample, kg/m^3.

2.2.5. Hydration products

After curing for a certain age, the sample was cut into thin slices of <3 mm, and then soaked in isopropanol (AR, 99.5 %) at a volume ratio of 1:10 for 24 h to terminate the hydration reaction of the sample (Chen et al., 2014; Snellings et al., 2018; Zhang and Scherer, 2011). After vacuum filtration, the sample was dried to constant weight in a vacuum drying oven at 45 °C. The dried sample was ground to <74 μm using a mortar for phase and thermogravimetric testing.

The phase composition of the sample was tested using an X-ray diffractometer (X-Ray Diffraction, XRD, Shimadzu 7000) with a scanning range of 5–90° 2θ and a scanning speed of 2°/min.

The thermogravimetric analysis of the sample was carried out using a Netzsch STA409PC thermal analyzer. About 20 mg of the sample was placed in an alumina crucible, heated from room temperature to 30 °C at a heating rate of 5 °C/min under a nitrogen atmosphere, held for 30 min, and then heated to 1000 °C at a heating rate of 15 °C/min to obtain the TG/DTG curve of the sample.

2.2.6. Compressive strength

The uniaxial compressive strength of the sample was tested after a certain curing period. After the sample was taken out of the curing box, the upper and lower surfaces were polished smooth to ensure good contact with the pressure machine. The test of uniaxial compressive strength was carried out using a Humboldt HM-5030 pressure machine with a loading rate of 1 mm/min. Five specimens of each mixture were tested and the average value was taken as the final compressive strength of the sample.

2.2.7. Pore structure

The pore size distribution was tested using a mercury porosimeter (Micromeritics' AutoPore IV 9500) in accordance with the ASTM D4404–18 standard. The maximum working pressure of the instrument is 414 MPa, and the pore size testing range is 3 nm ~ 1000 μm. A small cube measuring 1 × 1 × 1 cm^3 was soaked in isopropanol for 3 days, and then dried in a vacuum drying oven at 40 °C for 24 h.

2.2.8. Water permeability

The water permeability of the samples was tested using the methods by (Chindaprasirt et al., 2007). Firstly, a 40 mm-high slice was cut from the middle of the cylinder samples and dried in a vacuum drying oven for 24 h. After that, a 25 mm thick epoxy resin was then attached to the surface of samples to avoid water leakage. A pressure of 0.2 MPa was used in the test. The total time and the amount of water were recorded after the permeation rate was constant. Darcy's law was then used to calculate the water permeability.

2.2.9. Density function theory calculations

The DFT calculation was performed using the CASTEP module in Materials studio 8.0 (Accelrys Inc.). The exchange functional uses PBE-GBA (Fernández-Martínez et al., 2008). The BFGS algorithm was used to optimize the atomic position (Vanderbilt, 1990). The interaction between electrons was described by ultra-soft pseudopotential (Vanderbilt, 1990). The convergence thresholds for interatomic force, internal stress and atomic displacement were set at 0.03 eV·A^{-1}, 0.05 GPa and 0.001A, respectively. The convergence threshold of the total energy change and the self-consistent iteration accuracy were set as 1.0 × 10^{-5} eV·$atom^{-1}$ and 1.0 × 10^{-6} eV· $atom^{-1}$, respectively. Based on the convergence test, the cut off energy used in the calculation was 400 eV. 2 × 2 × 1 Monkhorst-Pack grid was used for sampling in Brillouin region. The adsorption energy (ΔE) can be calculated via Eq. (6):

$$\Delta E = E_{(surface+adsorbate)} - \left(E_{surface} + E_{adsorbate}\right) \quad (6)$$

where, $E_{(surface+adsorbate)}$ is the total energy after adsorption, eV; $E_{surface}$ and $E_{adsorbate}$ are the energy of the surface and adsorbate, respectively, eV.

3. Results and discussion

3.1. Sequential extraction procedure

The effect of HNTs and BC on the chemical fractions of As in BAW samples was shown in Fig. 4. As can be seen from Fig. 4, AW contained a small amount of water-soluble As, approximately 0.05 %, and its mid acido-

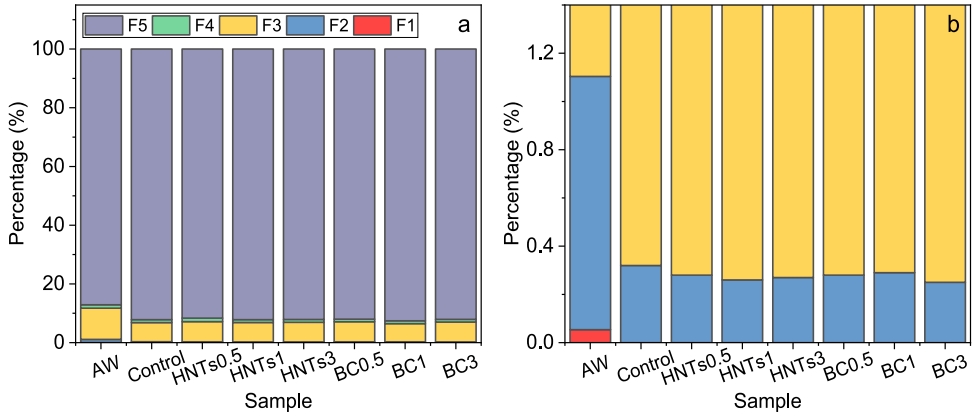

Fig. 4. Influence of HNTs and BC on the chemical fraction of As in BAW.

soluble fraction was as high as 1.05 %, resulting in a high As leaching amount.

After preparing cementitious materials using AW as raw material, the water-soluble As disappeared, and the content of other chemical fractions of As changed significantly. This was mainly due to a series of chemical changes that occur during the hydration process of the cementitious material. Compared with AW, the mid acido-soluble fraction in the control sample decreased to about 0.32 %, while the residual fraction increased to about 92.15 %.

water-soluble fraction (F1), mid acido-soluble fraction (F2), reducible fraction (F3), oxidizable fraction (F4), residual fraction (F5).

3.2. Leaching characteristics

The effect of HNTs and BC on the leaching concentration and immobilization rate of As was shown in Fig. 5. As shown in Fig. 5a, the leaching concentration of As in the control sample was as high as 1.08 mg/L, which far exceeded the requirement for As leaching amount in GB/T 14848–2017 (< 0.05 mg/L). The corresponding immobilization rate of As was only 50.7 %.

The addition of HNTs significantly reduced the leaching concentration of As. When 0.5 wt% HNTs was added, the leaching concentration of As was about 0.19 mg/L. Compared with the control sample, the leaching concentration of As decreased by about 82.4 %. Increasing the amount of HNTs further reduced the leaching concentration of As. At 1.0 wt% of HNTs, the leaching concentration of As reduced to around 0.15 mg/L, and the immobilization rate achieved approximately 90.9 %. This was related to the fact that HNTs to a certain extent reduced the content of mid acido-soluble fraction As. However, further increasing the amount of HNTs did not further improve the immobilization effect of As.

The addition of BC has also reduced the leaching concentration of As to a certain extent, but the effect of low-dose BC was not significant. As shown in Fig. 5, when the BC dosage was <3.0 wt%, it did not significantly affect the chemical binding state of As. Since the leaching behavior of As was directly affected by its chemical fraction, the effect of low-dose BC on As leaching was not significant. When the biochar dosage reached 3 wt%, the leaching concentration of As was reduced to about 0.08 mg/L, which was about 92.6 % lower than the control sample, and the immobilization rate of As was about 96.3 %, which was better than the same dosage of HNTs.

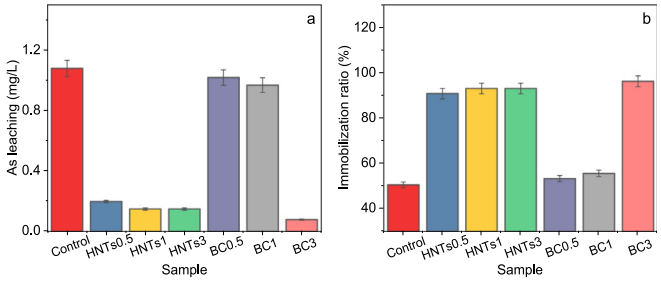

Fig. 5. Influence of HNTs and BC on the leaching concentration of As (a) and the immobilization ratio (b) in TCLP test.

Fig. 6 shows the effect of HNTs and BC on the leaching amount of As in the samples over time. Overall, the leaching concentration of As in each sample increased with leaching time. Fig. 6a shows the effect of HNTs on the leaching concentration of As. The addition of HNTs significantly reduced the leaching amount of As in each leaching cycle. In addition, when the HNTs content exceeded 1.0 wt%, the change in As leaching amount was not significant, which was consistent with the results of the TCLP test. Fig. 6b shows the effect of BC on the leaching concentration of As. Unlike HNTs, low BC content did not significantly affect the leaching amount of As.

According to the As leaching concentration, a double logarithmic curve ($lg(M_t)$-$lg(t)$) of the total leaching amount of As with leaching time was drawn, and the results were shown in Fig. 7. The data obtained were fitted and the results were shown in Table S3. As shown in Table S3, the cumulative leaching total amount (M_t) of the control sample during the entire leaching period (91d) was approximately 18.34 mg/m^2. The introduction of HNTs and BC reduced the M_t value. Incorporating 0.5 wt%, 1.0 wt%, and 3.0 wt% of HNTs resulted in M_t values of 8.48 mg/m^2, 3.18 mg/m^2, and 2.85 mg/m^2 for the respective samples, which were reduced by approximately 53.76 %, 82.66 %, and 84.46 % compared with the control sample. When 0.5 wt%, 1.0 wt%, and 3.0 wt% of BC were added, the M_t values of the samples were 15.92 mg/m^2, 11.31 mg/m^2, and 2.52 mg/m^2, respectively, which were reduced by approximately 13.12 %, 38.33 %, and 86.26 % compared with the control sample. This once again proved the inhibitory effect of HNTs and BC on As leaching.

According to the study by Van der Sloot H., the slope of the $lg(M_t)$-$lg(t)$ diagram can be used to determine the leaching mechanism of elements (van der Sloot and de Groot, 1990). If the slope is close to 0.5, then the leaching mechanism of the element is diffusion. If the slope is close to 0, then the leaching mechanism is surface wash-off, and if the slope is close to 1, then the leaching is controlled by dissolution (van der Sloot and de Groot, 1990). As shown in Table S5, the slope of the $log(M_t)$-$log(t)$ curve for all samples was close to 0.5, indicating that the release mechanism of As from BAW under these conditions was controlled by diffusion. This is consistent with the results of the previous studies by Zhang et al. (2020) and Gao et al. (2020), who used steel slag-based cementitious materials to solidify As-containing waste residues and studied the semi-dynamic leaching characteristics of As and found that the leaching of As was controlled by the diffusion.

Fig. 8 showed the CFL-$t^{\frac{1}{2}}$ relationship, and after fitting the data, a linear relationship was found between the two variables. The fitting parameters were shown in Table S4. The diffusion coefficient (D_e) of As was also calculated and was presented in Table S4. From Table S4, the diffusion

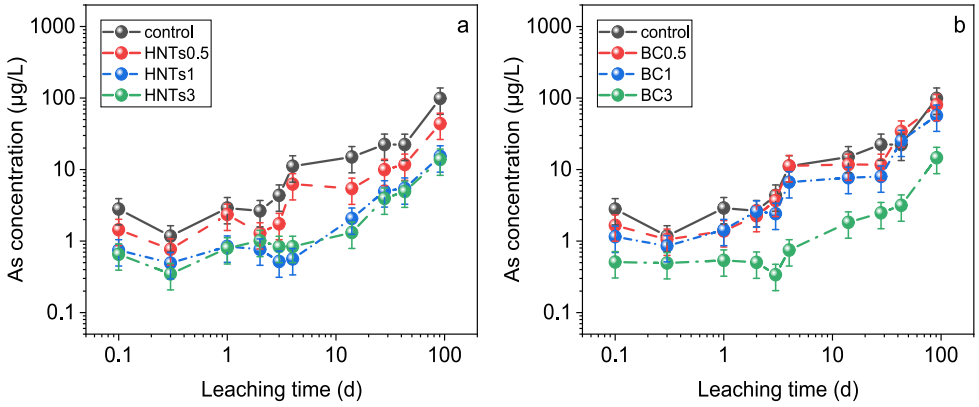

Fig. 6. The influence of HNTs and BC on the As leaching concentration from BAW with time: the influence of HNTs (a) and BC (b).

coefficient of As in BAW samples ranged between 10^{-15} and 10^{-16} cm^2/s. Based on the reports by Malviya and Chaudhary (2006), when the diffusion coefficient is $<3 \times 10^{-9}$ cm^2/s, the activity of harmful elements in the solidified material is low and can be applied in certain scenarios for the solidification of harmful elements, such as roadbeds, landfill sites, and quarry restoration. Under these conditions, the environmental risk value is within an acceptable range. Therefore, from this point of view, all tested samples met the relevant environmental requirements. In addition, as shown in Table S4, the diffusion coefficient of As in the control sample was the highest, about 6.58×10^{-15} cm^2/s, indicating the highest activity of As in it, which corresponds to the experimental results of higher As leaching in the control sample. Among the samples with HNTs and BC, BC3 had the lowest diffusion coefficient of As, about 1.24×10^{-16} cm^2/s.

The leaching index (*LI*) of As in the samples was calculated, and the results were shown in Table S4. If the leaching index is >9, the solidification process is considered effective (Zhang et al., 2020). According to Table S4, the leaching index values were approximately between 14 and 16, indicating that the solidification of As in BAW was effective. The leaching index values increased upon adding HNTs and BC, indicating that the immobilization capacity of BAW on As was improved. Thus, it can be inferred that the presence of HNTs and BC strengthened the solidification effect of BAW on As by reducing As's diffusion coefficient during the BAW leaching process.

3.3. Compressive strength

The effect of HNTs and BC on the compressive strength of BAW samples is shown in Fig. 9. As can be seen from Fig. 9, the addition of HNTs did not cause a significant impact on the compressive strength of BAW at 3d and 28d. A slight increase in compressive strength was observed for the lower content of HNTs, but when the content of HNTs reached 3.0 wt%, the compressive strength of BAW samples decreased slightly at 3d and 28d.

A small amount of BC slightly increased the early strength of BAW. Compared with the control sample, the compressive strength of BAW increased by about 9.36 % and 11.78 % at 0.5 wt% and 1 wt% biomass char content, respectively, after 3 days. After 28 days of curing, the compressive strength of BAW increased by about 3.38 % and 5.41 % at the same BC content, consistent with previous studies (Legan et al., 2022). Gupta et al. (2018) found that adding BC could significantly increase the compressive strength of samples. The fine particles in BC could act as nucleating agents for early hydration gel formation, promoting the reaction; furthermore, BC could also help to increase the density of the cured sample, and the synergistic effect of both promoted the strength growth of BAW samples.

However, as shown in Fig. 9, high content of BC (3.0 wt%) significantly reduced its early compressive strength. Compared with the control sample, the compressive strength of BAW decreased by about 30 % at 3.0 wt% BC content after 3 days. This is similar to the research results of Qin et al. (2021), which found that the compressive strength of the sample decreased

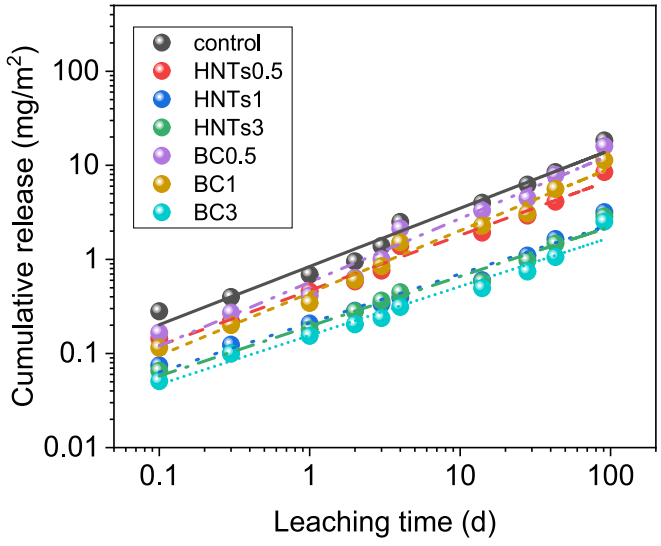

Fig. 7. The influence of HNTs and BC on the cumulative mass release of As from BAW.

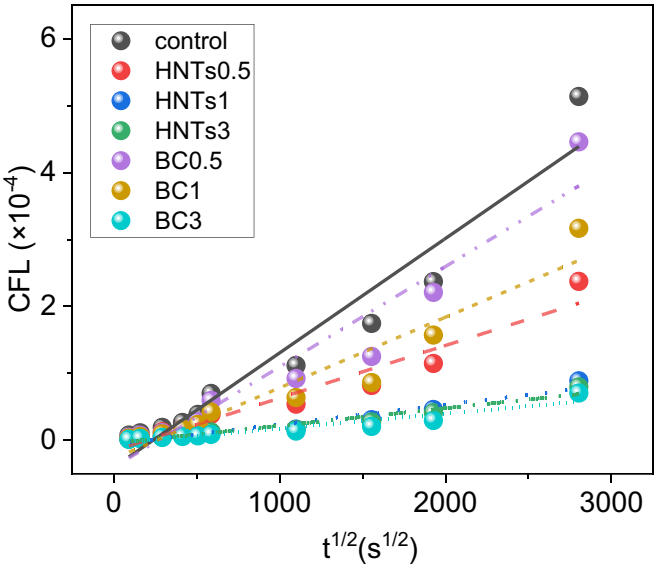

Fig. 8. The plot of $t^{1/2}$-*CFL*.

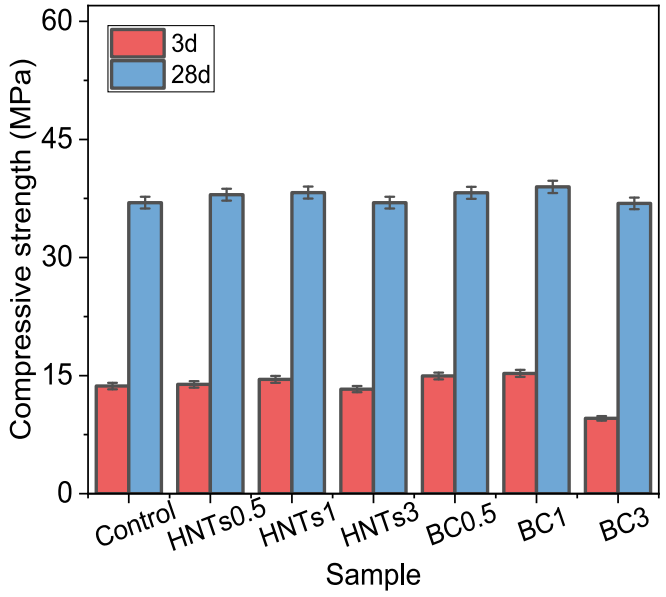

Fig. 9. The influence of chemical additives on the compressive strength of BAW.

when the BC content exceeded 0.65 wt%. This is likely due to excessive BC aggregation that hindered the reaction. Although the addition of 3.0 wt % BC significantly reduced the leaching concentration of As in BAW, its low early strength is likely to limit the practice utilization of BAW, at the same time, increasing the amount of BC will increase the BAW cost. Therefore, BC is seemed to unsuitable as an additive to optimize the solidification effect of As in BAW.

3.4. Reaction products

The influence of HNTs and BC on the products of BAW hydration reaction was shown in Figs. 10 and 11. Fig. 10 presents the TG results of the effects of HNTs and BC on the reaction products of BAW hydration after 3 and 28 days. It is found that the reaction products mainly consist of C-(A)-S-H, ettringite, and residual gypsum. Compared with the control sample, the addition of HNTs and a small amount of BC slightly increased the peak intensity around 130 °C in the DTG curve, indicating an increase in the generation of C-(A)-S-H and ettringite. This is consistent with the phenomenon of the early compressive strength increase of BAW samples with the addition of HNTs and a small amount of BC.

However, when the amount of BC reached 3 wt%, as shown in Fig. 10c and d, the generation of reaction products seemed to be significantly inhibited. The peak intensity around 130 °C in the DTG curve decreased significantly, indicating the inhibition of the generation of C-(A)-S-H and ettringite. At the same time, the peak intensity around 150 °C increased significantly, indicating an increase in the residual amount of gypsum. These results are consistent with the lower early strength of sample BC3. Obviously, a large amount of BC inhibited the progress of the reaction, hindered the formation of reaction gel, and thus reduced the early strength of the sample. After curing for 28 days, as shown in Fig. 10e-h, the addition of HNTs and BC did not have a significant effect on the production of hydration products.

Fig. 11 shows the XRD analysis results of the hydration products of BAW after 28 days of reaction. As shown in Fig. 11, similar to the results of TG analysis, the reaction products were mainly C-(A)-S-H and ettringite, with a small amount of residual gypsum. In addition, the addition of HNTs and BC did not change the phase composition of the BAW reaction products.

3.5. Microstructure

SEM results of the hydrated binders after curing for 28 days were shown in Fig. 12. It can be seen from Fig. 12a~c that there were many rodlike and

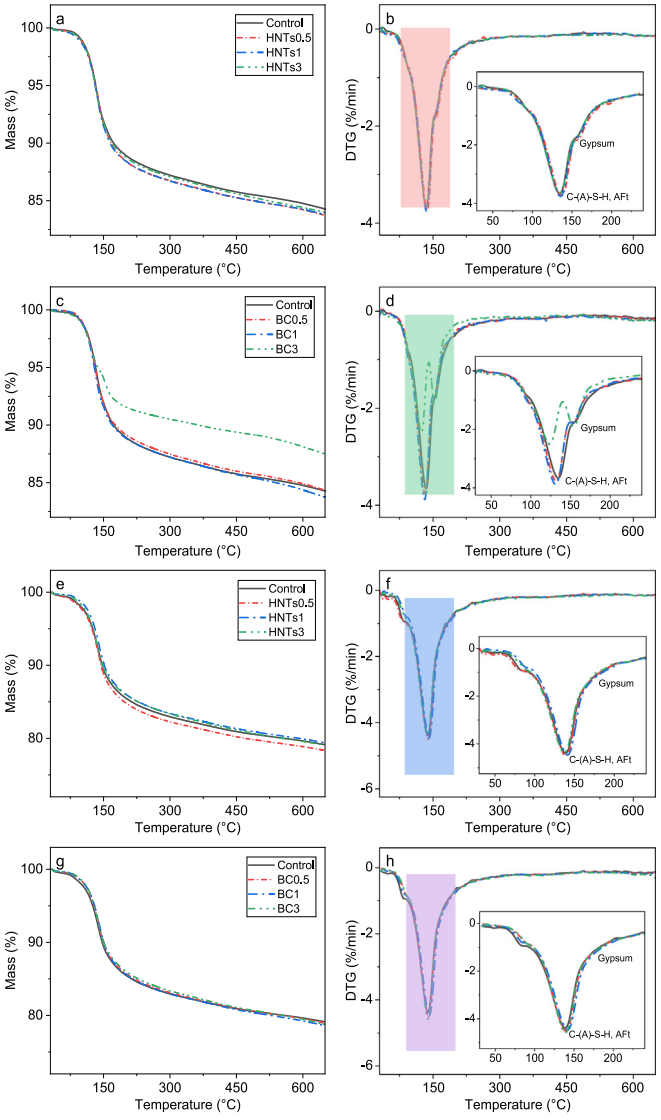

Fig. 10. TG analysis of the BAW samples after curing for 3 days (a-d) and 28 days (e-h).

irregular shape gels, which could be identified as ettringite and C-(A)-S-H, respectively, in line with the XRD and TG results. According to Fig. 12d~f and g ~ i, the addition of HNTs and BC did not strongly change the reaction gels. Needle-like HNTs could be found to distribute in the matrix, which served as fillers and favored a more compact structure, contributing to a better immobilization capacity.

4. Further discussion

4.1. Comparation between HNTs and BC

As has been discussed above, compared with the control sample, the addition of HNTs and BC slightly reduced the content of mid acido-soluble fraction, indicating that some As may be adsorbed by HNTs and BC, thereby reducing its activity. Among the chemical fractions of hazardous elements, water-soluble and mid acido-soluble fraction are more active and easily leached. In contrast, the residual fraction of hazardous elements has the highest "inertness" and better stability. Therefore, after being prepared into cementitious materials, the stability of As was enhanced.

Clay minerals are mainly layered silicate minerals, which are mainly distributed in soil and sediments. Common clay minerals include kaolinite, montmorillonite, illite, and chlorite. The layered silicate structure of clay

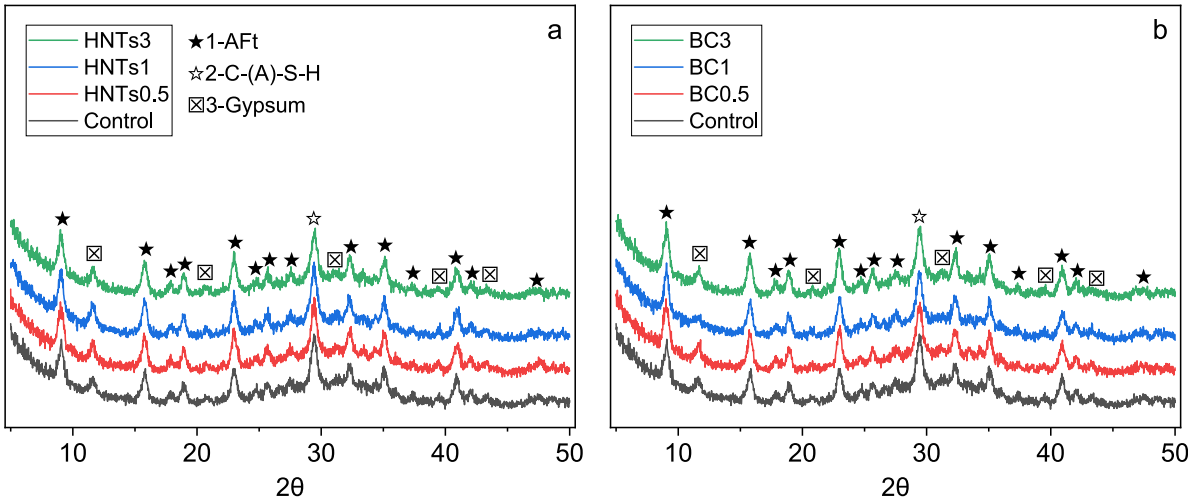

Fig. 11. XRD analysis of the BAW samples influenced by HNTs (a) and BC (b) after curing for 28 days.

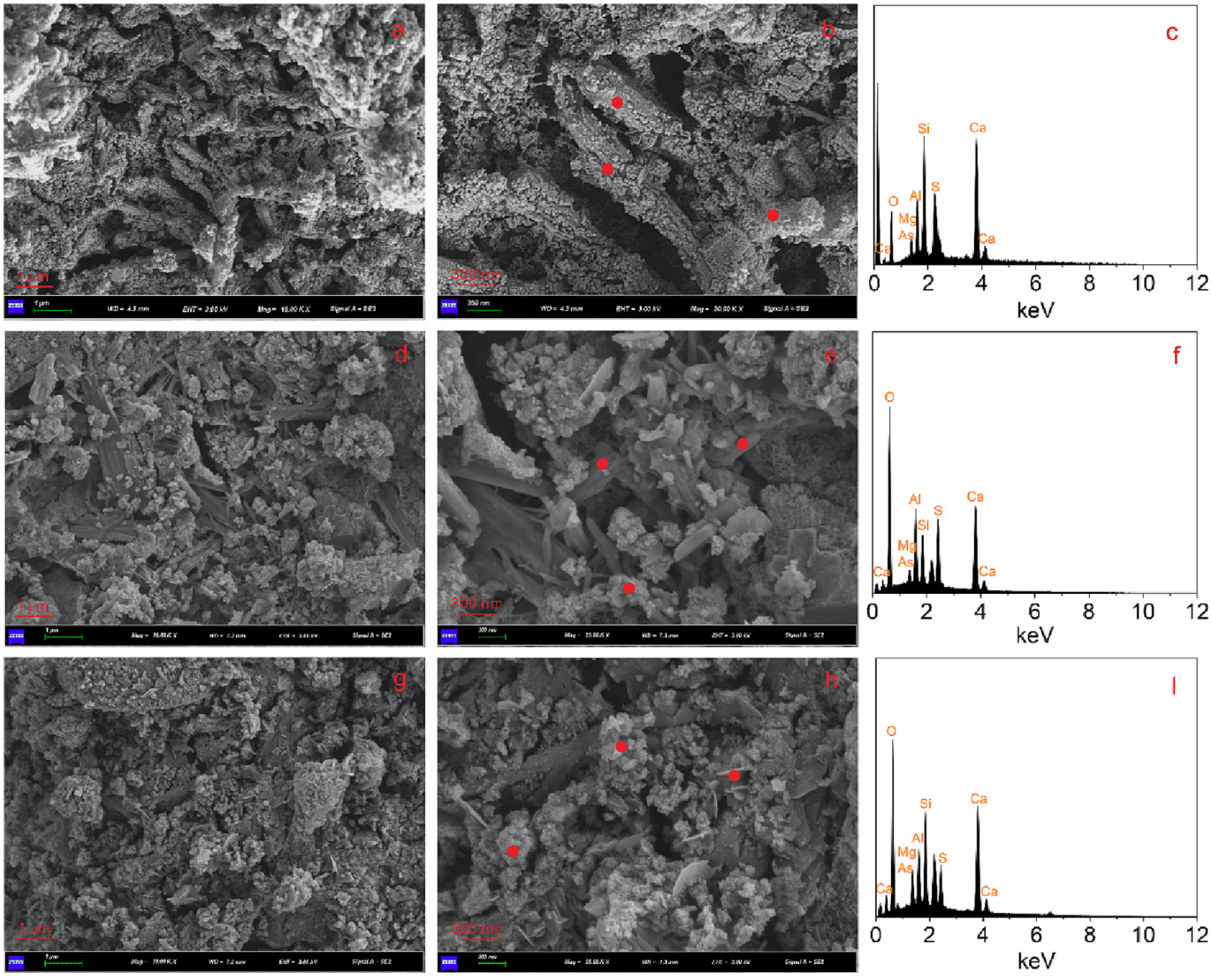

Fig. 12. SEM analysis of the BAW samples after curing for 28 days: (a ~ c) Control, (d ~ f) HNTs1, (h ~ i) BC.

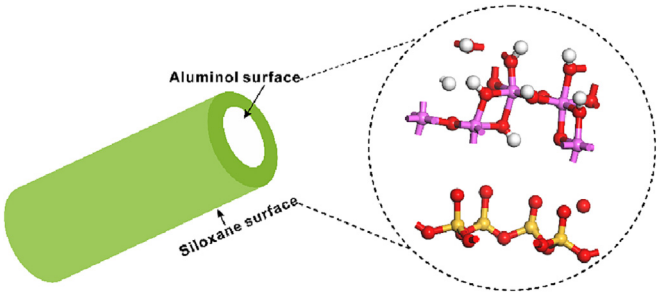

Fig. 13. Structure of HNTs.

minerals is mainly composed of Si—O tetrahedra and Al—O octahedra. According to the ratio of the two, clay minerals can be divided into 1:1 type and 1:2 type, among which kaolinite is a 1:1 type silicate mineral. HNTs are a kind of natural nanoscale clay mineral with a tubular structure. It can be regarded as a special kind of kaolinite with a structural formula of $Al_2(OH)_4Si_2O_5{\cdot}nH_2O$, where n = 1–2. The outer surface of the tubular structure of HNTs is composed of Si—O groups, and the Al—O groups are located on the inner surface of its nanotube cavity, as shown in Fig. 13. Compared with Si—O, the Al—O on its inner surface has higher chemical activity. Considering the special structure of HNTs, in the present work, it is believed that part of the As species could be adsorbed by HNTs, and then decreased its leaching amount.

Biochar is a type of biomass generated by anaerobic decomposition or incomplete combustion of carbon-rich materials such as agricultural waste (straw, rice straw, and rice husk, etc.), municipal solid waste, and livestock waste (Wang et al., 2012). Due to its high specific surface area, high porosity, and surface-enriched active groups such as -COOH, -OH, and C═O, biochar has been widely used in soil improvement, restoration of heavy metal-polluted soil, and other fields. Previous studies have found that biochar can alter the distribution and forms of heavy metals in contaminated soil, increase the stability of heavy metals, and thus have a good immobilization effect on heavy metals. Fan (2020) found that under certain conditions, biochar can reduce the adsorption of As by soil particles and promote the effectiveness of As in soil, which has a certain influence on the migration ability of As in soil environment. Ni (2015) studied the fixation effects of different biochars on lead and As and found that corn char had a certain adsorption and immobilization effect on As, but iron-loaded corn char had a better immobilization effect on As, which was 13 times that of corn char. The adsorption mechanism of biochar on As can be explained by Fig. 14. On the one hand, the surface functional groups of biochar can form complexes and hydrogen bonds with As species. On the other hand, the oxygen-containing functional groups (such as phenol-OH, C═OH, etc.) on the surface of biochar can act as electron acceptors to oxidize trivalent As into pentavalent As (Sharma et al., 2022). Since trivalent As has higher activity and toxicity than pentavalent As, this reduces the toxicity and activity of As.

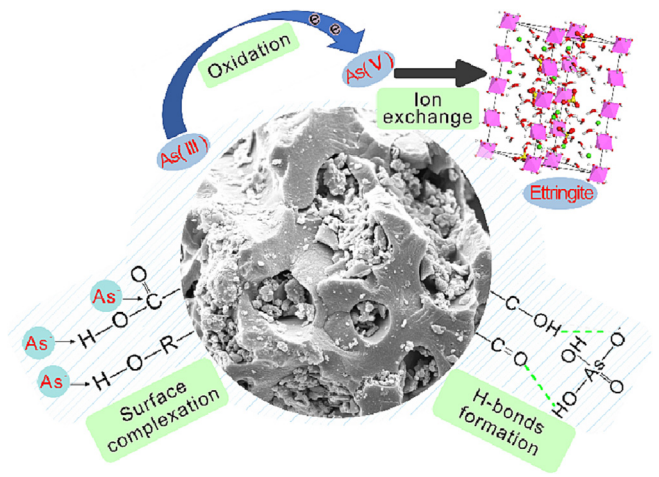

Fig. 14. The immobilization mechanism of As by BC.

Although higher amount of BC could effectively increase the As immobilization capacity of BAW, the presence of excess BC strongly decreased the compressive strength of BAW especially at the early curing ages (Fig. 9). As a result, BC is not suitable to be used in this situation.

The decrease in compressive of BAW caused by BC could be attributed to the restriction of BC on the binder hydration. During the reaction process of BAW, under the attacking of the alkaline environment, the elements such as Si and Al in slag are leached out, while the SO_4^{2-} in AW begins to release and generates gel materials mainly composed of C-(A)-S-H and ettringite (Fig. 15). Therefore, the leaching rate of Si, Al, and SO_4^{2-}, that is, the dissolution rate of BFS and AW, plays a crucial role in the progress of the reaction. BC is rich in hydroxyl groups (-OH) on its surface, which aggregate on the surface of reactant particles to form hydrogen bonds and connect with each other through water molecules to form hydrophilic groups (Huang et al., 2019). These hydrophilic groups form a stable water film that hinders the dissolution of raw materials and thus inhibits the progress of the reaction. The greater the amount of BC, the thicker the water film, and the more obvious the inhibitory effect on the reaction. In this experiment, the addition of 3.0 wt% of BC may lead to the formation of a dense water film on the surface of BFS and AW, hindering the progress of the reaction and inhibiting the production of reaction products. The compressive strength evolution of BAW was then limited.

4.2. The chemical stabilization effects of HNTs

DFT calculation was used in the present work to explain the chemical stabilization effects of HNTs on As. In the present work, H_3AsO_3 and H_4AsO_4 were used to represent the As(III) and As(V) species. The modes of the surface and As species used for the calculation were shown in Fig. S3. According to the difference of O atom in the Al-OH surface, there are four types of adsorption modes for both As(III) and As(V) species, as shown in Fig. 16. The calculated adsorption energy was also shown in Fig. 16. It can be seen from Fig. 16 that all the adsorption energies were negative values, ranging from −0.63 ~ −1.68 eV for As(III) species, and − 0.98 ~ −1.63 eV for As(V) species, suggesting that both As(III) and As(V) species could be adsorbed on the surface of HNTs surface through the formation of surface H-bonds. As a result, one of the reasons for the decrease in the As leaching concentration from BAW in the presence of HNTs could be attributed to the adsorption of As species onto the surface of HNTs.

4.3. The physical encapsulation effects of HNTs

Fig. 17 shows the effect of HNTs on the pore structure of BAW. As shown in Fig. 17a, the pores of BAW are mainly distributed between 3–100 nm, and the presence of HNTs had a significant impact on the pore structure. As shown in Fig. 17b and Table 1, adding HNTs reduced the cumulative pore area (CPA) of BAW. When adding 0.5 wt%, 1.0 wt%, and 3.0 wt% HNTs, the CPA value of BAW was reduced to 87.61 m^2/g, 82.38 m^2/g, and 79.81 m^2/g, respectively, with reductions of about 25.34 %, 29.81 %, and 32.00 %.

HNTs optimized the pore structure of the BAW, reduce the porosity, and thus lower the leaching of As. Therefore, the physical aspects of HNTs on As immobilization effects of BAW was related to the optimization of the pore structure achieved through physical filling, which made the entire matrix denser. In addition, as explored in Section 3.2, the leaching of As was controlled by diffusion, which is the mass transfer from the matrix to the external solution, and largely depends on the porosity of the matrix (Tang et al., 2020). Therefore, the reduction of CPA weakens the diffusion ability of As, thereby enhancing the immobilization capacity of BAW.

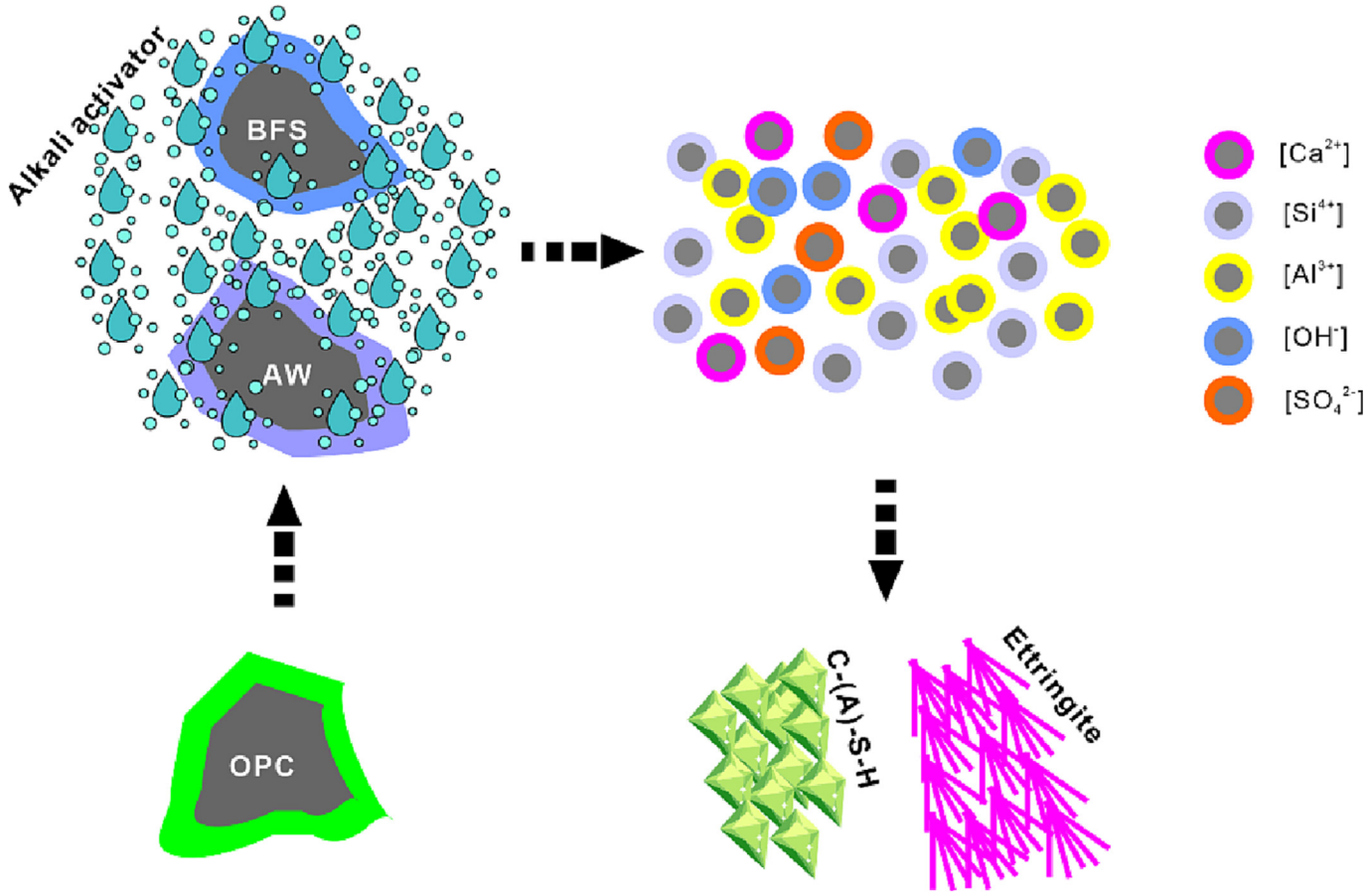

Fig. 15. Reaction mechanism of BAW.

5. Conclusion

The present work explored the feasibility of using halloysite nanotubes and biochar to modify the As immobilization capacity of a binder prepared from AW through experiments and DFT calculations. Based on the results, the following conclusions can be drawn:

(1) The addition of both HNTs and BC could increase the immobilization capacity of BAW for As species. The effect of BC only was observed in its high dosage, reaching 3 wt%, however, high amount of BC strongly decreased the early age strength of BAW. By contrast, the addition of HNTs did not lead to significant changes on the strength development of BAW.

(2) Based on the DFT calculation results, the chemical effects of HNTs on As immobilization were the adsorption of As species onto the surface of HNTs through the formation of H-bonds.

(3) The physical encapsulation effects of BAW on As species increased due to the addition of HNTs. This was because the pore structure of BAW became more refined through the filling effects of HNTs particles, resulting in a denser matrix.

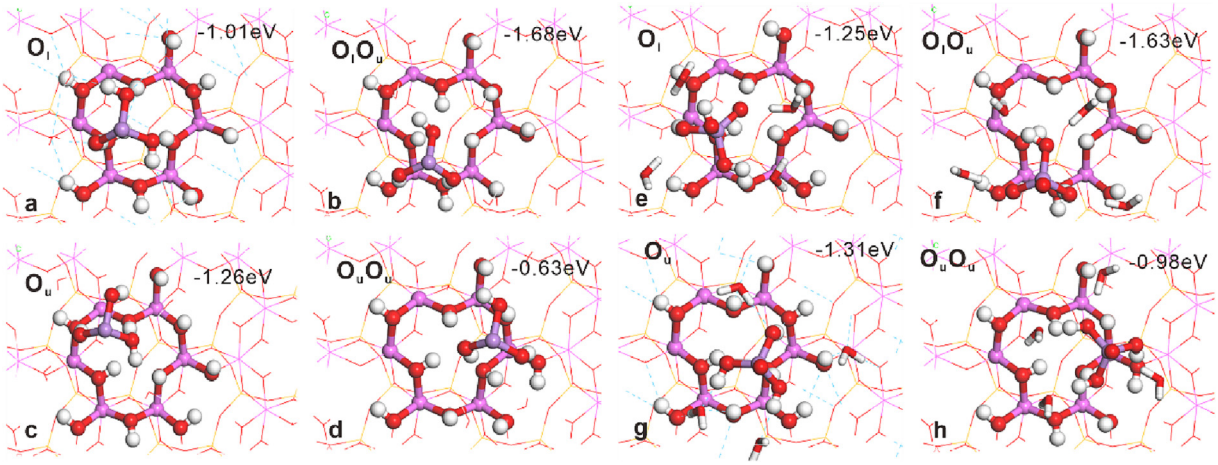

Fig. 16. Adsorption of arsenic species onto the surface of HNTs: (a ~ d) As(III), (e ~ f) As(V).

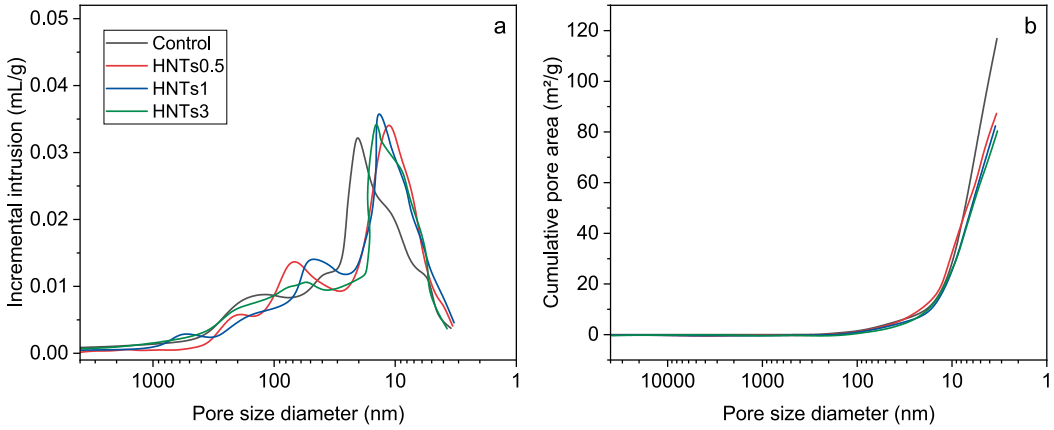

Fig. 17. The influence of chemical additives on the pore structure of BAW at 28 days: (a) pore size distribution, (b) total pore area.

Table 1
Total pore area (CPA) of BAW after curing for 28 days (m^2/g).

Samples	Control	HNTs-0.5	HNTs-1	HNTs-3
CPA	117.36	87.61	82.38	79.81

CRediT authorship contribution statement

Yingliang Zhao: Data curation, Writing- Original draft preparation. **Jingping Qiu**: Conceptualization, Methodology. **Xiaogang Sun and Zhenbang Guo**: Supervision. **Yong Sun**: Visualization, Investigation.

Data availability

Data will be made available on request.

Declaration of competing interest

The authors declare that they have no known competing financial interests or personal relationships that could have appeared to influence the work reported in this paper.

Acknowledgements

The authors would like to thank the supports from National Natural Science Foundation of China (Key Program), 52234004. Moreover, the authors would like to thank Yao Fan from Shiyanjia Lab (www.shiyanjia.com) for the cloud computing services.

Appendix A. Supplementary data

Supplementary data to this article can be found online at https://doi.org/10.1016/j.scitotenv.2023.164637.

References

Alias, S.S., Harun, Z., Abu, Mansor S., 2020. Characterization and performance of rice husk as additive in green ceramic water filter fabricated by slip-casting. WJE 17 (4), 553–562.
Arrascue, M.E.L., van Niekerk, J., 2006. Biooxidation of arsenopyrite concentrate using BIOX® process: industrial experience in Tamboraque, Peru. Hydrometallurgy 83 (1–4), 90–96. https://www.sciencedirect.com/science/article/pii/S0304386X06000776.
Avalos, N.M., Varga, T., Mergelsberg, S.T., Silverstein, J.A., Saslow, S.A., 2021. Behavior of iodate substituted ettringite during aqueous leaching. Appl. Geochem. 125, 104863.
Baldermann, A., Preissegger, V., Šimić, S., Letofsky-Papst, I., Mittermayr, F., Dietzel, M., 2021. Uptake of aqueous heavy metal ions (Co2+, Cu2+ and Zn2+) by calcium-aluminium-silicate-hydrate gels. Cem. Concr. Res. 147, 106521.
Basu, A., Mahata, J., Gupta, S., Giri, A.K., 2001. Genetic toxicology of a paradoxical human carcinogen, arsenic: a review. Mutat. Res. Rev. Mutat. Res. 488 (2), 171–194. https://www.sciencedirect.com/science/article/pii/S1383574201000564.
Brierley, J.A., 2003. Response of microbial systems to thermal stress in biooxidation-heap pretreatment of refractory gold ores. Hydrometallurgy 71 (1–2), 13–19. https://www.sciencedirect.com/science/article/pii/S0304386X03001439.
Cao, B., Fan, S., Tan, X., Li, M., Hu, Y., 2017. Cementitious materials modified with hematite nanoparticles for enhanced cement hydration and uranium immobilization. Environ. Sci. Nano 4 (8), 1670–1681.
Cataldo, S., Lazzara, G., Massaro, M., Muratore, N., Pettignano, A., Riela, S., 2018. Functionalized halloysite nanotubes for enhanced removal of lead(II) ions from aqueous solutions. Appl. Clay Sci. 156, 87–95.
Che, J., Zhang, W., Ma, B., Chen, Y., Wang, L., Wang, C., 2022. A shortcut approach for cooperative disposal of flue dust and waste acid from copper smelting: decontamination of arsenic-bearing waste and recovery of metals. Sci. Total Environ. 843, 157063. https://www.sciencedirect.com/science/article/pii/S0048969722041602.
Chen, X., Meawad, A., Struble, L.J., 2014. Method to stop geopolymer reaction. J. Am. Ceram. Soc. 97 (10), 3270–3275.
Chen, L., Wang, L., Zhang, Y., Ruan, S., Mechtcherine, V., Tsang, D.C., 2022. Roles of biochar in cement-based stabilization/solidification of municipal solid waste incineration fly ash. Chem. Eng. J. 430, 132972. https://www.sciencedirect.com/science/article/pii/S1385894721045484.
Chen, L., Nakamura, K., Hama, T., 2023. Review on stabilization/solidification methods and mechanism of heavy metals based on OPC-based binders. J. Environ. Manag. 332, 117362. https://www.sciencedirect.com/science/article/pii/S0301479723001500.
Chindaprasirt, P., Homwuttiwong, S., Jaturapitakkul, C., 2007. Strength and water permeability of concrete containing palm oil fuel ash and rice husk–bark ash. Constr. Build. Mater. 21 (7), 1492–1499. https://www.sciencedirect.com/science/article/pii/S0950061806001334.
Chrysochoou, M., Dermatas, D., 2006. Evaluation of ettringite and hydrocalumite formation for heavy metal immobilization: literature review and experimental study. J. Hazard. Mater. 136 (1), 20–33.
Dandautiya, R., Singh, A.P., Kundu, S., 2018. Impact assessment of fly ash on ground water quality: an experimental study using batch leaching tests. Waste Manag. Res. 36 (7), 624–634.
Dias, Y.N., Pereira, Wendel Valter, da Silveira, Da, Costa, M.V., de Souza, E.S., Ramos, S.J., Amarante, Cbd, et al., 2022. Biochar mitigates bioavailability and environmental risks of arsenic in gold mining tailings from the eastern Amazon. J. Environ. Manag. 311, 114840. https://www.sciencedirect.com/science/article/pii/S0301479722004133.
Emmanuel, E., Yong, L.L., Anggraini, V., Pasbakhsh, P., 2020. Can halloysite nanotubes be used to remediate zinc and lead-contaminated marine clay? A solidification/stabilization approach. Appl. Clay Sci. 186, 105441.
Fan, J., 2020. Activation Mechanisms and Application of Biochar on Arsenic in Soil. Master. Taiyuan.
Fan, S., Cao, B., Deng, N., Hu, Y., Li, M., 2019. Effects of ferrihydrite nanoparticle incorporation in cementitious materials on radioactive waste immobilization. J. Hazard. Mater. 379, 120570.
Fernández-Martínez, A., Cuello, G.J., Johnson, M.R., Bardelli, F., Román-Ross, G., Charlet, L., et al., 2008. Arsenate incorporation in gypsum probed by neutron, X-ray scattering and density functional theory modeling. J. Phys. Chem. A 112 (23), 5159–5166.
Gao, W., Ni, W., Zhang, Y., Li, Y., Shi, T., Li, Z., 2020. Investigation into the semi-dynamic leaching characteristics of arsenic and antimony from solidified/stabilized tailings using metallurgical slag-based binders. J. Hazard. Mater. 381, 120992.
Gillispie, E.C., Mergelsberg, S.T., Varga, T., Webb, S.M., Avalos, N.M., Snyder, M.M.V., et al., 2021. Competitive TcO4-, IO3-, and CrO42- incorporation into Ettringite. Environ. Sci. Technol. 55 (2), 1057–1066.
Gong, H., Zhao, L., Rui, X., Hu, J., Zhu, N., 2022. A review of pristine and modified biochar immobilizing typical heavy metals in soil: applications and challenges. J. Hazard. Mater. 432, 128668.
Guo, L., Du, Y., Yi, Q., Li, D., Cao, L., Du, D., 2015. Efficient removal of arsenic from "dirty acid" wastewater by using a novel immersed multi-start distributor for sulphide feeding. Sep. Purif. Technol. 142, 209–214. https://www.sciencedirect.com/science/article/pii/S1383586614007746.
Guo, B., Liu, B., Yang, J., Zhang, S., 2017. The mechanisms of heavy metal immobilization by cementitious material treatments and thermal treatments: a review. J. Environ. Manag. 193, 410–422.

Gupta, S., Kua, H.W., Koh, H.J., 2018. Application of biochar from food and wood waste as green admixture for cement mortar. Sci. Total Environ. 619-620, 419–435.
Halim, C.E., Amal, R., Beydoun, D., Scott, J.A., Low, G., 2003. Evaluating the applicability of a modified toxicity characteristic leaching procedure (TCLP) for the classification of cementitious wastes containing lead and cadmium. J. Hazard. Mater. 103 (1), 125–140. https://www.sciencedirect.com/science/article/pii/S0304389403002450.
Hamid, Y., Tang, L., Hussain, B., Usman, M., Rehman Hashmi, M.L.U., Bilal Khan, M., et al., 2020. Immobilization and sorption of Cd and Pb in contaminated stagnic anthrosols as amended with biochar and manure combined with inorganic additives. J. Environ. Manag. 257, 109999.
He, M., Xu, Z., Hou, D., Gao, B., Cao, X., Ok, Y.S., et al., 2022. Waste-derived biochar for water pollution control and sustainable development. Nat. Rev. Earth Environ. 3 (7), 444–460.
HJ 557–-2010, 2010. Solid waste—Extraction procedure for leaching toxicity—Horizontal vibration method: Ministry of Environmental Protection of the People's Republic of China.
Huang, Y., Xu, C., Li, H., Jiang, Z., Gong, Z., Yang, X., et al., 2019. Utilization of the black tea powder as multifunctional admixture for the hemihydrate gypsum. J. Clean. Prod. 210, 231–237.
Irisawa, K., Namiki, M., Taniguchi, T., Garcia-Lodeiro, I., Kinoshita, H., 2022. Solidification and stabilization of strontium and chloride ions in thermally treated calcium aluminate cement modified with or without sodium polyphosphate. Cem. Concr. Res. 156, 106758.
Kushwaha, R., Singh, R.S., Mohan, D., 2023. Comparative study for sorption of arsenic on peanut shell biochar and modified peanut shell biochar. Bioresour. Technol. 375, 128831. https://www.sciencedirect.com/science/article/pii/S0960852423002572.
Lagno, F., Rocha, S.D.F., Chryssoulis, S., Demopoulos, G.P., 2010. Scorodite encapsulation by controlled deposition of aluminum phosphate coatings. J. Hazard. Mater. 181 (1–3), 526–534. https://www.sciencedirect.com/science/article/pii/S0304389410006291.
Langhans, D., Lord, A., Lampshire, D., Burbank, A., Baglin, E., 1995. Biooxidation of an arsenic-bearing refractory gold ore. Miner. Eng. 8 (1–2), 147–158. https://www.sciencedirect.com/science/article/pii/089268759400109P.
Legan, M., Gotvajn, A.Ž., Zupan, K., 2022. Potential of biochar use in building materials. J. Environ. Manag. 309, 114704.
Li, L., Wang, F., Lv, Y., Liu, J., Zhang, D., Shao, Z., 2018. Halloysite nanotubes and Fe3O4 nanoparticles enhanced adsorption removal of heavy metal using electrospun membranes. Appl. Clay Sci. 161, 225–234. https://www.sciencedirect.com/science/article/pii/S0169131718301522.
Li, Y., Zhu, X., Qi, X., Shu, B., Zhang, X., Li, K., et al., 2020. Removal and immobilization of arsenic from copper smelting wastewater using copper slag by in situ encapsulation with silica gel. Chem. Eng. J. 394, 124833.
Lin, Y., Hu, X., Zi, F., Chen, Y., Chen, S., Li, X., et al., 2022. Rapid gold cyanidation from a sulfur-high and arsenic-high micro-fine concentrate via facile two-stage roasting pretreatment. Miner. Eng. 190, 107938. https://www.sciencedirect.com/science/article/pii/S0892687522005489.
Mahallei, H., Badv, K., 2021. The study of diffusion characteristics of soil bentonite to control contaminant transport. WJE 18 (3), 379–388.
Malviya, R., Chaudhary, R., 2006. Leaching behavior and immobilization of heavy metals in solidified/stabilized products. J. Hazard. Mater. 137 (1), 207–217.
Mehrotra, V.P., Sai, A., Kapur, P.C., 1982. Plaster of Paris activated supersulfated slag cement. Cem. Concr. Res. 12 (4), 463–473. https://www.sciencedirect.com/science/article/pii/0008884682900618.
Mohanty, S.K., Valenca, R., Berger, A.W., Yu, I.K., Xiong, X., Saunders, T.M., et al., 2018. Plenty of room for carbon on the ground: potential applications of biochar for stormwater treatment. Sci. Total Environ. 625, 1644–1658. https://www.sciencedirect.com/science/article/pii/S0048969718300378.
Ni, Q., 2015. Immobilization of Lead and Arsenic by Biochars. Master. Hangzhou.
Nunan, T.O., Viana, I.L., Peixoto, G.C., Ernesto, H., Verster, D.M., Pereira, J.H., et al., 2017. Improvements in gold ore cyanidation by pre-oxidation with hydrogen peroxide. Miner. Eng. 108, 67–70. https://www.sciencedirect.com/science/article/pii/S0892687517300158.
Ouhadi, V.R., Yong, R.N., Deiranlou, M., 2021. Enhancement of cement-based solidification/stabilization of a lead-contaminated smectite clay. J. Hazard. Mater. 403, 123969.
Peng, B., Lei, J., Min, X.-B., Chai, L.-Y., Liang, Y.-J., You, Y., 2017. Physicochemical properties of arsenic-bearing lime–ferrate sludge and its leaching behaviors. Trans. Nonferrous Metals Soc. China 27 (5), 1188–1198.
Phenrat, T., Marhaba, T.F., Rachakornkij, M., 2008. Leaching behaviors of arsenic from arsenic-iron hydroxide sludge during TCLP. J. Environ. Eng. 134 (8), 671–682.
Qin, Y., Pang, X., Tan, K., Bao, T., 2021. Evaluation of pervious concrete performance with pulverized biochar as cement replacement. Cem. Concr. Compos. 119, 104022. https://www.sciencedirect.com/science/article/pii/S0958946521000913.
Quedou, P.G., Wirquin, E., Bokhoree, C., 2021. A sustainable approach in using construction and demolition waste materials in concrete. WJE 18 (6), 826–840.
Randall, P., Chattopadhyay, S., 2004. Advances in encapsulation technologies for the management of mercury-contaminated hazardous wastes. J. Hazard. Mater. 114 (1–3), 211–223. https://www.sciencedirect.com/science/article/pii/S0304389404004194.
Sharma, P.K., Kumar, R., Singh, R.K., Sharma, P., Ghosh, A., 2022. Review on arsenic removal using biochar-based materials. Groundw. Sustain. Dev. 17, 100740.
van der Sloot, H., de Groot, G.H., 1990. Determination of Leaching Characteristics of Waste Materials in Relation to Environmental Product Certification.
Snellings, R., Chwast, J., Cizer, Ö., de Belie, N., Dhandapani, Y., Durdzinski, P., et al., 2018. Report of TC 238-SCM: hydration stoppage methods for phase assemblage studies of blended cements—results of a round robin test. Mater. Struct. 51 (4), 1.
Straif, K., Benbrahim-Tallaa, L., Baan, R., Grosse, Y., Secretan, B., El Ghissassi, F., et al., 2009. A review of human carcinogens—part C: metals, arsenic, dusts, and fibres. Lancet Oncol. 10 (5), 453–454. https://www.sciencedirect.com/science/article/pii/S1470204509701342.
Stueckle, T.A., Lu, Y., Davis, M.E., Wang, L., Jiang, B.-H., Holaskova, I., et al., 2012. Chronic occupational exposure to arsenic induces carcinogenic gene signaling networks and neoplastic transformation in human lung epithelial cells. Toxicol. Appl. Pharmacol. 261 (2), 204–216. https://www.sciencedirect.com/science/article/pii/S0041008X12001317.
Sun, X., Li, J., Sun, X., Zheng, J., Wu, Z., Liu, W., et al., 2021. Efficient stabilization of arsenic in the arsenic-bearing lime-ferrate sludge by zero valent iron-enhanced hydrothermal treatment. Chem. Eng. J. 421, 129683.
Tang, P.-P., Zhang, W.-L., Chen, Y.-H., Chen, G., Xu, J., 2020. Stabilization/solidification and recycling of sediment from Taihu Lake in China: engineering behavior and environmental impact. Waste Management (New York, N.Y.). vol. 116, pp. 1–8.
Vanderbilt, 1990. Soft self-consistent pseudopotentials in a generalized eigenvalue formalism. Phys. Rev. B 41 (11), 7892–7895.
Wang, D., Wang, Q., 2022. Clarifying and quantifying the immobilization capacity of cement pastes on heavy metals. Cem. Concr. Res. 161, 106945.
Wang, H., Feng, Y., Chen, Y., 2012. Advances in biochar production from wastes and its applications. Chem. Ind. Eng. Prog. 31 (04), 907–914.
Wang, L., Chen, L., Tsang, D.C., Kua, H.W., Yang, J., Ok, Y.S., et al., 2019. The roles of biochar as green admixture for sediment-based construction products. Cem. Concr. Compos. 104, 103348.
Wang, Q., Li, J.-S., Xue, Q., Poon, C.S., 2022. Immobilization and recycling of contaminated marine sediments in cement-based materials incorporating iron-biochar composites. J. Hazard. Mater. 435, 128971.
Xu, H., Min, X., Wang, Y., Ke, Y., Yao, L., Liu, D., et al., 2020. Stabilization of arsenic sulfide sludge by hydrothermal treatment. Hydrometallurgy 191, 105229.
Yang, D., Sasaki, A., Endo, M., 2019a. Reclamation of a waste arsenic-bearing gypsum as a soil conditioner via acid treatment and subsequent Fe(II) As stabilization. J. Clean. Prod. 217, 22–31. https://www.sciencedirect.com/science/article/pii/S0959652619302136.
Yang, D., Sasaki, A., Endo, M., 2019b. Reclamation of an arsenic-bearing gypsum via acid washing and CaO-As stabilization involving svabite formation in thermal treatment. J. Environ. Manag. 231, 811–818. https://www.sciencedirect.com/science/article/pii/S0301479718312611.
Yu, I.K.M., Xiong, X., Tsang, D.C.W., Wang, L., Hunt, A.J., Song, H., et al., 2019. Aluminium-biochar composites as sustainable heterogeneous catalysts for glucose isomerisation in a biorefinery. Green Chem. 21 (6), 1267–1281.
Zhang, J., Scherer, G.W., 2011. Comparison of methods for arresting hydration of cement. Cem. Concr. Res. 41 (10), 1024–1036.
Zhang, M., Yang, C., Zhao, M., Yu, L., Yang, K., Zhu, X., et al., 2018. Immobilization of Cr(VI) by hydrated Portland cement pastes with and without calcium sulfate. J. Hazard. Mater. 342, 242–251.
Zhang, Y., Gao, W., Ni, W., Zhang, S., Li, Y., Wang, K., et al., 2020. Influence of calcium hydroxide addition on arsenic leaching and solidification/stabilisation behaviour of metallurgical-slag-based green mining fill. J. Hazard. Mater. 390, 122161.
Zhang, W., Che, J., Wen, P., Xia, L., Ma, B., Chen, J., et al., 2021. Co-treatment of copper smelting flue dust and arsenic sulfide residue by a pyrometallurgical approach for simultaneous removal and recovery of arsenic. J. Hazard. Mater. 416, 126149. https://www.sciencedirect.com/science/article/pii/S0304389421011134.
Zhang, H., Zhao, Y., Hou, D., Hao, H., 2022a. Cementitious binders modified with halloysite nanotubes for enhanced lead immobilization. Powder Technol. 395, 149–157.
Zhang, Y., He, M., Wang, L., Yan, J., Ma, B., Zhu, X., et al., 2022b. Biochar as construction materials for achieving carbon neutrality. Biochar 4 (1), 59.
Zhao, J., Luo, Q., Ding, L., Fu, R., Zhang, F., Cui, C., 2022a. Valency distributions and geochemical fractions of arsenic and antimony in non-ferrous smelting soils with varying particle sizes. Ecotoxicol. Environ. Saf. 233, 113312. https://www.sciencedirect.com/science/article/pii/S014765132200152X.
Zhao, Y., Gu, X., Qiu, J., Zhang, S., Guo, Z., Sun, X., 2022b. Recycling of arsenic-containing biohydrometallurgy waste to produce a binder for cemented paste backfill: co-treatment with oil shale residue. J. Environ. Manag. 319, 115621.
Zhao, Y., Gu, X., Qiu, J., Zhang, S., Guo, Z., Sun, X., 2022c. Recycling of arsenic-containing biohydrometallurgy waste to produce a binder for cemented paste backfill: influence of additives. J. Clean. Prod. 132515.
Zhao, Y., Qiu, J., Zhang, S., Guo, Z., Wu, P., Sun, X., et al., 2022d. Recycling of arsenic-containing biohydrometallurgy waste to produce a binder for cemented paste backfill: mix proportion optimization. Powder Technol. 398, 117155.